Critical thickness for transformation of epitaxially stabilized cubic AlN in superlattices

I. W. Kim, Quan Li, L. D. Marks, and S. A. Barnett[a)]
Department of Materials Science and Engineering, Northwestern University, Evanston, Illinois 60208

(Received 26 July 2000; accepted for publication 12 December 2000)

The epitaxial stabilization and transformation of cubic AlN layers in AlN/VN and AlN/TiN superlattices, grown by reactive sputtering on MgO (001), is described. In AlN/VN, the critical AlN thickness l^C for transformation from cubic to hexagonal increased from ≈3.0 to >4 nm when the VN superlattice layer thickness was increased from 2.0 to 6.0 nm. The effect of lattice mismatch was observed by comparing AlN/VN (mismatch = 1.46%) and AlN/TiN (mismatch = 3.84%). The l^C values were smaller, 2–2.5 nm, for the larger mismatch AlN/TiN system. The dependence of l^C on the lattice mismatch and stabilizing layer thickness is discussed based on models of epitaxial stabilization. © *2001 American Institute of Physics.* [DOI: 10.1063/1.1345831]

Epitaxial stabilization of nonequilibrium phases in monolithic thin films has been well documented.[1,2] There are a number of examples, such as α-Sn[3,4] and zincblende GaN,[5] where relatively thick stabilized layers can be grown. However, in many other cases the critical thickness l^C beyond which the layer transforms to the stable state is very small, limiting potential applications of stabilized materials. Recently, epitaxial stabilization in superlattices has been used to obtain thick films containing many thin stabilized layers, yielding novel properties. Examples include nitride superlattice hard coatings[6] and magnetic superlattices.[7,8] While l^C has been measured in a number of different stabilized monolithic films,[9] relatively few data are available for superlattices. This is true for example in Co/Cu, where l^C has been determined for metastable fcc Co thin films on Cu substrates[9] but not in Co/Cu superlattices. Epitaxial stabilization in a superlattice structure is different than in a thin film on a thick substrate. During superlattice growth, the stabilized layer nucleates on a series of layers with comparable thicknesses, yielding a different strain state than for a single layer on a substrate. The thicknesses of both layers of the superlattice, as well as their lattice constants, can thus affect the stabilization.

Perhaps the most detailed characterization of l^C has been done in nitride superlattices, e.g., AlN/TiN [10] and $CrN_{0.6}$/TiN,[11] where AlN and $CrN_{0.6}$ (normally hexagonal) were stabilized in the cubic rocksalt structure. l^C was determined as a function of period, but the effect of varying the relative superlattice layer thicknesses was not investigated. Another factor that has not been studied is the coherency strain due to lattice mismatch. While the contribution of coherency strain to the energy of an epitaxially stabilized layer has been discussed,[12] there is no experimental data regarding its effect on l^C. In a study of AlN stabilization in AlN/NbN,[13] where the mismatch is large (7.4%), it was difficult to determine the effect of coherency strain because of lattice relaxation, defects, and nonplanar growth.

In this letter, experimental results on the stabilization of B1-cubic AlN and its transformation to the stable wurtzite structure are presented. We describe the effect of VN layer thickness in AlN/VN superlattices. The effect of lattice mismatch was studied by comparing AlN/VN, with mismatch = 1.5% (a_{VN} = 0.414 nm, a_{B1-AlN} ≈ 0.408 nm), and AlN/TiN with mismatch = 3.84% (a_{TiN} = 0.424 nm).

Epitaxial superlattices were deposited on MgO (001) using ultrahigh vacuum reactive magnetron sputter deposition[14] in Ar–N_2 (99.999% purity) mixtures. 5-cm-diam V (or Ti) and Al targets (99.95% purity) were used. For AlN/VN, a total pressure of 15 mTorr and a nitrogen partial pressure of 3–4 mTorr yielded stoichiometric nitrides. For AlN/TiN, a lower nitrogen partial pressure of 2–3 mTorr yielded stoichiometric films, presumably due to the higher heat of formation of TiN (338 kJ/mole) and AlN (318 kJ/mole) compared to that of VN (218 kJ/mole). Good quality AlN/VN superlattices were obtained at lower temperatures (550–700 °C) than for AlN/TiN (650–800 °C). This was apparently due to the lower melting temperature of VN (2320 °C) compared to TiN (2950 °C), and the smaller lattice mismatch between B1–AlN and B1–VN compared to B–1 AlN and B1–TiN. 50-nm-thick VN buffer layers were grown on the MgO substrates prior to the AlN/VN. According to the Matthews–Blakeslee criterion,[15] the VN layer should be 92% relaxed at this thickness. On the other hand, AlN/TiN superlattices were grown directly on MgO, since it has a lattice constant almost identical to TiN.

A multilayer sample was prepared for cross-sectional transmission electron microscopy (XTEM) that contained three consecutively grown superlattices with different AlN layer thicknesses: $[AlN(1.8\,nm)/VN(6.3\,nm)]_3$, $[AlN(4.1\,nm)/VN(6.3\,nm)]_3$, and $[AlN(8.1\,nm)/VN(6.3\,nm)]_3$. After cross sectioning,[16] the structures were examined in a 200 kV cold-field-emission-gun transmission electron microscope (TEM). Figure 1(a) shows a high resolution XTEM image and diffraction pattern taken from the $[AlN(4.1\,nm)/VN(6.2\,nm)]_3$ portion. The image was taken with the electron beam along the [001] direction. The lattice fringes retain a square symmetry throughout the image, and the diffraction pattern in the inset verifies the cubic symmetry. Figure 1(b) shows a high resolution

[a)]Author to whom correspondence should be addressed; electronic mail: s-barnett@nwu.edu

Downloaded 22 Nov 2006 to 129.105.122.65. Redistribution subject to AIP license or copyright, see http://apl.aip.org/apl/copyright.jsp

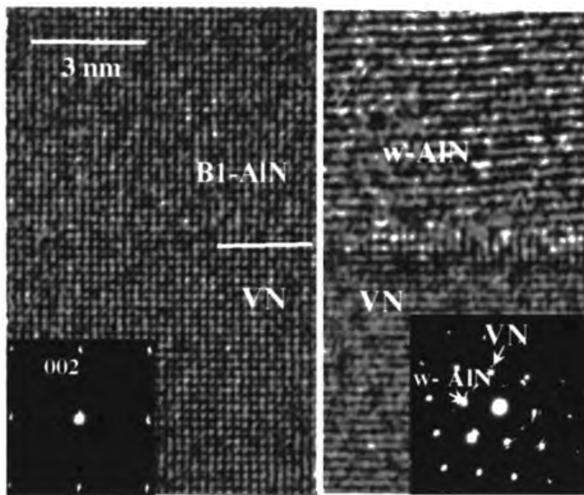

FIG. 1. High resolution electron microscope images from different portions of an AlN/VN multilayer. (a) First 4.1-nm-thick AlN layer grown, and a portion of the underlying VN. (b) First 8.1-nm-thick AlN layer grown, and the underlying VN. The selected-area diffraction patterns, shown in the insets, were taken from the corresponding three-period stacks.

XTEM image and diffraction pattern from the $[AlN(8.1\,nm)/VN(6.2\,nm)]_3$ portion. The lattice fringes in the AlN layer show a spacing that matches w-AlN (0001) rather than B1–AlN. Elongated spots in the diffraction pattern were identified as w-AlN (100) and (120) and B1–VN (110), indicating a transformation to the wurtzite structure and a change in film orientation. Note that these orientations were also observed in XTEM images in layers grown after the w-AlN (not shown here).

Figure 2 shows the XRD results from (a) $[AlN(2.7\,nm)/VN(2.0\,nm)]_{45}$, (b) $[AlN(3.0\,nm)/VN(2.0\,nm)]_{45}$, and (c) $[AlN(4.0\,nm)/VN(6.2\,nm)]_{45}$ superlattices. The x-ray diffraction (XRD) scans were carried out in a double-crystal diffractometer equipped with a LiF focusing monochromator. The VN (002) peaks are from the VN buffer layer. For $l_{AlN}=2.7$ nm, the substrate, superlattice, and buffer-layer Bragg reflections were present, with no other peaks. A kinematical high-angle XRD computer simulation assuming a trapezoidal composition modulation[17] was used to fit the data. The best fit in Fig. 2(a) was obtained by assuming B1–AlN and B1–VN layers with interfacial widths of 0.3 nm and layer thickness fluctuations of 0.2–0.25 nm, similar to prior results for B1–AlN/B1–TiN superlattices.[10] The fits yielded lattice spacings of 0.405 ± 0.002 nm for B1–AlN and 0.413 ± 0.003 nm for VN, in agreement with bulk values within error.[18] For $l_{AlN} = 3.0$ nm, the predominant peaks were a broad w-AlN (0002) reflection, a superlattice Bragg (002) reflection, and a cubic VN (002) reflection from the VN buffer layer. No high-angle satellite reflections were visible and the superlattice Bragg peak was weak [≈ 7 times lower intensity than in Fig. 2(a)]. The peaks expected for a good quality epitaxial superlattice, generated using the simulation and shown for comparison in Fig. 2(b), do not agree with the experimental data. Thus, the AlN has at least partially transformed to wurtzite with a (0002) texture, and the layered structure has been lost. These results show that the transition to wurtzite occurs at $l^C = 2.7-3.0$ nm for 2-nm-thick VN layers.

For the $[AlN(4.0\,nm)/VN(6.2\,nm)]_{45}$ superlattice in

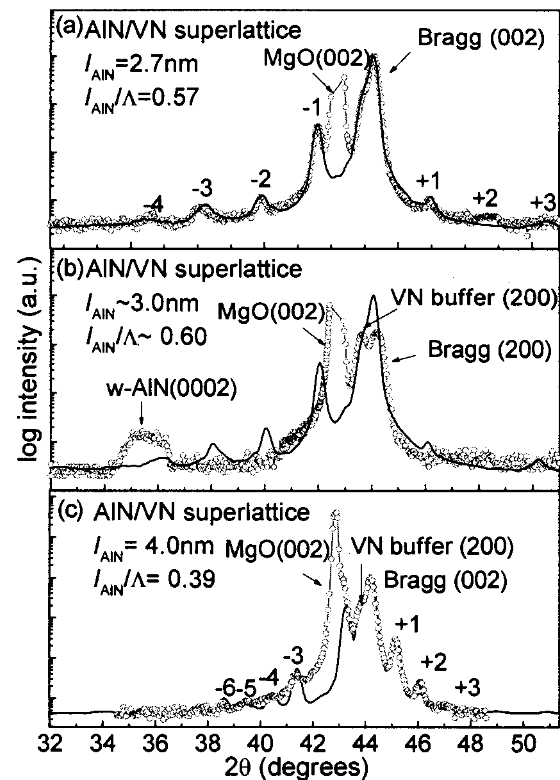

FIG. 2. High angle x-ray diffraction θ–2θ scans from AlN/VN superlattices: (a) $[AlN(2.7\,nm)/VN(2.0\,nm)]_{45}$, $l_{AlN}/\Lambda = 0.57$; (b) $[AlN(3.0\,nm)/VN(2.0\,nm)]_{45}$, $l_{AlN}/\Lambda = 0.60$, and (c) $[AlN(4.0\,nm)/VN(6.2\,nm)]_{45}$, $l_{AlN}/\Lambda = 0.39$. The simulated patterns obtained by assuming high-quality cubic layered structures are shown for comparison (—•— experimental, —— simulated).

Fig. 2(c), the pattern shows only substrate and buffer layer Bragg peaks along with superlattice reflections. An excellent fit was obtained by assuming B1–AlN and using parameters similar to those used in Fig. 2(a). l^C was thus >4 nm for 6.2-nm-thick VN layers, substantially larger than for 2-nm-thick VN. This increase in AlN critical thickness with increasing VN layer thickness can be rationalized as follows. If the AlN layer exceeds the VN layer in thickness, there may be insufficient VN to maintain stabilization. In this case, rather than imposing its structure on the AlN, the VN may be deformed by the transforming AlN; note that there is a 23% volume expansion associated with the transformation. Indeed, in $CrN_{0.6}$/TiN superlattices deposited at low temperatures,[11] highly deformed zones were observed in the TiN layers within ≈ 5 nm of the interfaces after the CrN transformed from cubic to hexagonal. [The deformation was presumably not observed in Fig. 1(b) because of the high growth temperature, which allowed annealing of defects.] Thus, decreasing the thickness of the VN layer decreases the amount of material that must be deformed during the transformation of AlN, decreasing the barrier to transformation, and hence the critical thickness.

Figure 3 shows a typical θ–2θ scan from a $[AlN(2.6\,nm)/TiN(4.5\,nm)]_{14}$ superlattice, with a similar layer-thickness ratio as that shown in Fig. 2(c). No distinct superlattice reflections can be identified in this pattern. The solid line in Fig. 3 is the simulated pattern that would be expected for a high-quality epitaxial superlattice. The marked disagreement with the experimental data clearly

Downloaded 22 Nov 2006 to 129.105.122.65. Redistribution subject to AIP license or copyright, see http://apl.aip.org/apl/copyright.jsp

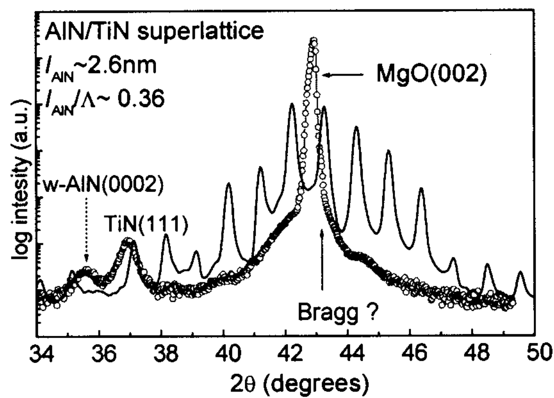

FIG. 3. A high angle x-ray diffraction θ–2θ scan from a $[AlN(2.6\ nm)/TiN(4.5\ nm)]_{14}$ superlattice. The simulated patterns obtained by assuming high-quality cubic layered structures are shown for comparison (—•— experimental, —— simulated).

shows that this was not a good superlattice. The predominant peaks were identified as w-AlN (0002) and TiN(111). This indicates that AlN had transformed to the wurtzite phase. In prior work, it was shown that AlN layers up to ≈2 nm thick were stabilized in the B1 structure.[10] Thus, the critical thickness for transformation of AlN in AlN/TiN superlattices was 2.0–2.5 nm, smaller than that in AlN/VN superlattices.

The dependence of l^C on lattice mismatch can be explained using a simple model accounting only for the AlN bulk[19] and interfacial energies. The total energy E_T per unit area of an AlN layer during growth is written

$$E_T=(E_B+E_S)l+E_I, \tag{1}$$

where E_B is the strain-free bulk energy, E_S is the coherency strain energy, E_I is the interfacial energy, and l is the thickness of the growing AlN layer. Writing Eq. (1) for both the B1 and wurtzite structures and equating the total energies yields l^C

$$l^C=(E_1^w-E_1^{B1})/[(E_B^{B1}-E_B^w)+(E_S^{B1}-E_S^w)]. \tag{2}$$

The l^C values can be compared for AlN/VN and AlN/TiN as follows. The E_I terms are expected to be roughly equal for AlN/VN and AlN/TiN interfaces, because of the very similar structure and bonding of VN and TiN. The E_B terms are fixed values for each of the AlN structures.[19] The wurtzite/B1 interface is likely incoherent, so the coherency strain E_S^w can be neglected. On the other hand, the B1/B1 interface is coherent for thin enough layers, so that E_S^{B1} depends on the mismatch. Switching from VN to TiN increases the coherency strain energy E_S^{B1}, and Eq. (2) shows that this decreases l^C.

The authors are grateful to Professor Peter Voorhees for useful discussions. This work was supported by the MRSEC program of the National Science Foundation, Grant No. DMR-9632472.

[1] R. Bruinsma and A. Zangwill, J. Phys. (France) **47**, 2055 (1986).
[2] D. M. Wood and A. Zunger, Phys. Rev. B **40**, 4062 (1989).
[3] M. T. Asom, A. R. Kortan, L. C. Kimerling, and R. C. Farrow, Appl. Phys. Lett. **55**, 1439 (1989).
[4] R. F. C. Farrow, D. S. Robertson, G. M. Williams, A. G. Cullis, G. R. Jones, I. M. Young, and P. N. J. Dennis, J. Cryst. Growth **54**, 507 (1981).
[5] J. W. Orton and C. T. Foxon, Rep. Prog. Phys. **61**, 1 (1998).
[6] M. Setoyama, A. Nakayama, M. Tanaka, N. Kitagawa, and T. Nomura, Surf. Coat. Technol. **225**, 86 (1997).
[7] M. J. Hall, B. J. Hickey, M. A. Howson, M. J. Walker, J. Xu, D. Greig, and N. Wiser, Phys. Rev. B **47**, 12785 (1993).
[8] F. J. Lamelas, C. H. Lee, H. He, W. Vavra, and R. Clarke, Phys. Rev. B **40**, 5837 (1989).
[9] M. T. Keif and W. F. Egelhoff, Phys. Rev. B **47**, 10785 (1993).
[10] A. Madan, I. W. Kim, S. C. Cheng, P. Yashar, V. P. Dravid, and S. A. Barnett, Phys. Rev. Lett. **78**, 1743 (1997).
[11] P. Yashar, X. Chu, S. A. Barnett, J. Rechner, Y. Y. Wang, M. S. Wong, and W. D. Sproul, Appl. Phys. Lett. **72**, 987 (1998).
[12] H. von Känel, C. Schwarz, S. Goncalves-conto, E. Muller, L. Miglio, F. Tavazza, and G. Malegori, Phys. Rev. Lett. **74**, 1163 (1995).
[13] A. Madan, I. W. Kim, M. Guruz, V. P. Dravid, and S. A. Barnett (unpublished).
[14] P. B. Mirkarimi, M. Shinn, and S. A. Barnett, J. Vac. Sci. Technol. A **10**, 1618 (1992).
[15] *Epitaxial Growth*, edited by J. W. Matthews (Academic, New York, 1975).
[16] Q. Li, S. A. Barnett, and L. D. Marks (unpublished).
[17] A. Madan, P. Yashar, M. Shinn, and S. A. Barnett, Thin Solid Films **302**, 147 (1997).
[18] Inorganic Index to the Powder Diffraction File, Joint Committee on Powder Diffraction Standards, Swathmore, Pennsylvania (1994).
[19] N. E. Christensen and I. Gorczyca, Phys. Rev. B **50**, 4397 (1994).

Downloaded 22 Nov 2006 to 129.105.122.65. Redistribution subject to AIP license or copyright, see http://apl.aip.org/apl/copyright.jsp